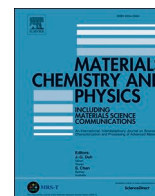| Title	Development of an equiatomic octonary TiNbTaZrMoHfWCr super-high-entropy alloy for biomedical applications
Author(s)	Matsuzaka, Tadaaki; Hyakubu, Akira; Kim, Yong Seong et al.
Citation	Materials Chemistry and Physics. 2024, 316, p. 129120
Version Type	VoR
URL	https://hdl.handle.net/11094/94897
rights	This article is licensed under a Creative Commons Attribution 4.0 International License.
Note	

Development of an equiatomic octonary TiNbTaZrMoHfWCr super-high-entropy alloy for biomedical applications

Tadaaki Matsuzaka [a], Akira Hyakubu [a], Yong Seong Kim [a], Aira Matsugaki [a], Takeshi Nagase [b], Takuya Ishimoto [a,c], Ryosuke Ozasa [a], Hyoung Seop Kim [d], Tomoji Mizuguchi [e], Ozkan Gokcekaya [a], Takayoshi Nakano [a,*]

[a] Division of Materials and Manufacturing Science, Graduate School of Engineering, Osaka University, 2-1 Yamadaoka, Suita, Osaka, 565-0871, Japan
[b] Department of Materials and Synchrotron Radiation Engineering, Graduate School of Engineering, University of Hyogo, 2167 Shosha, Himeji, Hyogo, 671-2280, Japan
[c] Aluminium Research Center, University of Toyama, 3190 Gofuku, Toyama, 930-8555, Japan
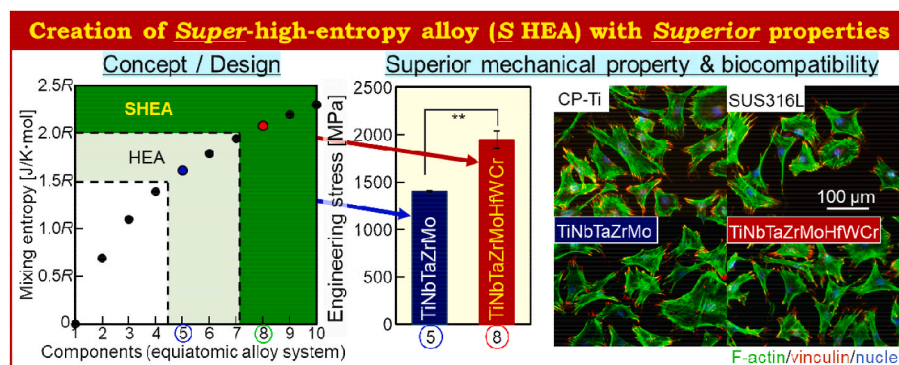[d] Department of Materials Science and Engineering, Pohang University of Science and Technology, Pohang, 37673, South Korea
[e] Advanced Technology & Strategy Department, Technology Group, JX Metals Corporation, 10-4 Toranomon 2-chome, Tokyo, 105-8417, Japan

HIGHLIGHTS

- A super-high-entropy alloy (SHEA) with $\Delta S_{\mathrm{mix}} > 2.0R$ was designed.
- Octonary TiNbTaZrMoHfWCr SHEA was developed for biomedical applications (BioSHEA).
- Biocompatibility of the BioSHEA was comparable to that of pure Ti.
- BioSHEA showed high yield strength (~2000 MPa) due to solid-solution strengthening.

GRAPHICAL ABSTRACT

ABSTRACT

A super-high-entropy alloy (SHEA) with $\Delta S_{\mathrm{mix}} \geq 2.0R$ (where R is the gas constant) was designed to produce metallic materials with superior mechanical properties to conventional alloys. As an alternative to conventional quinary high-entropy alloys (HEAs), herein, octonary SHEAs for biomedical applications (BioSHEAs) are proposed for the first time, and the TiNbTaZrMoHfWCr BioSHEA was fabricated. Arc-melted BioSHEA exhibited an extremely high yield strength of 1953 ± 84 MPa, which was approximately 550 MPa higher than that of the quinary TiNbTaZrMo BioHEA. This yield strength is considerably higher than that estimated by the rule of mixtures for pure metals, confirming the achievement of significant solid-solution strengthening induced by a supermulticomponent solid solution composed of elements with different atomic radii. Its biocompatibility was comparable to that of pure Ti and the quinary BioHEA, and superior to that of SUS316L. This study demonstrates

* Corresponding author. Division of Materials and Manufacturing Science, Graduate School of Engineering, Osaka University, 2-1 Yamadaoka, Suita, Osaka, 565-0871, Japan.
E-mail address: nakano@mat.eng.osaka-u.ac.jp (T. Nakano).

the validity of a novel entropy-based guideline for increasing the mixing entropy to achieve metallic materials with ultrahigh strength.

1. Introduction

In recent years, high-entropy alloys (HEAs) have attracted increasing attention from both academia and industry as a new class of metallic materials that exhibit sophisticated mechanical functionality. HEAs with an extremely large number of elemental combinations and compositions have been reported. For these alloys, the formation of a solid solution (solid-solution strengthening) based on increased mixing and/or configurational entropy (ΔS_{mix}) is the foundation of their properties, and in some cases, various precipitates and separated phases have been utilized to successfully develop excellent mechanical properties. Based on the success with increasing the mixing entropy (multi-componentization), it has been suggested that increasing the mixing entropy to more than that in ordinary HEAs could be beneficial for achieving even higher functionality in metallic materials. A further increase in the number of mixing elements (~10 elements), (and consequently, a further increase in the mixing entropy) has been shown to improve solid-solution strengthening [1,2] owing to an increase in lattice strain [2]. The greater variation in composition [3] may also promote HEA-specific nonlinear effects. However, the super-multicomponent alloys reported in previous studies contain harmful elements such as Ni and Co, because they are often developed for refractory applications.

This study proposes *super*-HEAs (SHEAs) for biomedical applications (BioSHEAs), which have an even higher mixing entropy ($\Delta S_{mix} \geq 2.0R$, where R is the gas constant) than HEAs ($\Delta S_{mix} \geq 1.5R$), to bring metallic biomaterials to a novel class with superior mechanical properties. The 'S' in the abbreviation of SHEA indicates both *super* and *superior*, which expresses the alloy's superior strength expected. To achieve $\Delta S_{mix} \geq 2.0R$, at least eight elements are required in the equiatomic alloy system (Fig. 1(a)).

We fabricated a BioHEA for the first time using only elements with low biotoxicity [4,5]. Subsequently, several researchers have developed and characterized new BioHEAs and medium-entropy ($1.0R \leq \Delta S_{mix} \leq 1.5R$) alloys for metallic biomaterials (BioMEAs) [6–14]. However, BioSHEA for biomaterials has not yet been reported. This study aimed to develop a novel BioSHEA consisting only of elements with low biotoxicity. Moreover, the potential of BioSHEA was explored by evaluating their mechanical and biological functionalities.

2. Materials and methods

Ingots of the TiNbTaZrMoHfWCr BioSHEA and TiNbTaZrMo BioHEA were prepared via arc melting (ACM-S01, DIAVAC Ltd., Japan) using mixed lumps of pure elements. The alloys were melted at least ten times and maintained in a liquid state for approximately 120 s during each melting event to ensure chemical composition homogeneity. The cooling rate during arc melting was reported to be approximately 2×10^3 K/s based on secondary dendrite spacing [15,16].

The constituent phases and microstructures were investigated using optical microscopy (OM; BX60, Olympus, Japan), X-ray diffraction (XRD; D8 DISCOVER, Bruker, Japan), energy-dispersive X-ray spectroscopy (EDS; Aztec 3.1, Oxford Instruments, UK), and field-emission scanning electron microscopy (FE-SEM; JIB-4610F, JEOL, Japan).

Rectangular specimens ($2 \times 2 \times 5$ mm) were prepared to characterize the mechanical properties by compression, and the 5 mm side was parallel to the compressive force. Compression tests (n = 3) were conducted using an Instron-type testing machine (AG-X, Shimadzu, Japan) at a nominal strain rate of 1.67×10^{-4} s^{-1} and room temperature. Nanoindentation hardness (ENT-1100, Elionix, Japan) was calculated using the Oliver and Pharr method [17].

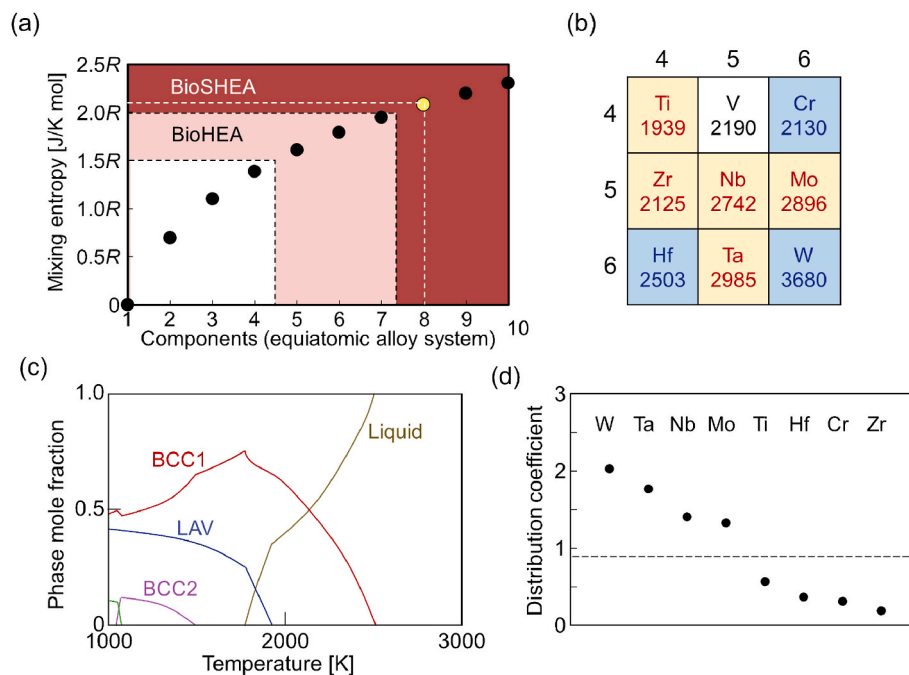To evaluate the biocompatibility, a cell culture experiment was

Fig. 1. Dependence of mixing entropy (ΔS_{mix}) on the number of constituent elements in the equiatomic alloy system. (a) Mixing entropy–number of constituent elements in the equiatomic alloy system. (b) Periodic table with melting temperatures including the elements involved in the SHEA design. (c) Equilibrium thermodynamic calculation results for TiNbTaZrMoHfWCr BioSHEA. (d) Distribution coefficients of the constituent elements of TiNbTaZrMoHfWCr BioSHEA at the liquidus temperature.

performed using a previously reported method [18]. Plate specimens (5 × 5 × 1 mm) were prepared from commercially pure Ti (CP–Ti), 316 L-type stainless steel (SUS-316L), and the TiNbTaZrMo alloy as reference materials, in addition to the TiNbTaZrMoHfWCr BioSHEA test specimens (n = 5). Primary osteoblasts were isolated from 3-day-old mouse calvariae, diluted to 8000 cells/cm^2, and cultured on the specimens for 24 h in a 5% CO_2 humidified atmosphere. Cell density was evaluated using Giemsa staining (FUJIFILM Wako Chemicals, Japan). Cell morphology was evaluated using immunocytochemistry. Quantitative results are expressed as the mean ± standard deviation values.

Statistical significance was evaluated using one-way analysis of variance (ANOVA), followed by Tukey's post-hoc test. A p-value <0.05 is considered statistically significant.

3. Results and discussion

Based on the equiatomic quinary TiNbTaZrMo BioHEA, an equiatomic octonary TiNbTaZrMoHfWCr BioSHEA was designed by adding Cr, Hf, and W (Fig. 1(b)). While choosing the elements for the BioSHEA, toxic elements were excluded based on IC$_{50}$ [19], which is a measure of biotoxicity. Furthermore, the following parameters, which are generally used in the design of BioHEAs, were used to select the elements: mixing enthalpy (ΔH_{mix}) for evaluating the atomic interactions among the constituent elements, δ for evaluating the difference in the atomic size of the constituent elements, a dimensionless parameter Ω, which is defined by the combination of the ΔS_{mix}, ΔH_{mix}, melting-temperature values of the pure elements, and valence electron concentration (VEC) [20–27].

The contribution of solid-solution strengthening to strength (yield strength, $\Delta\sigma$) was estimated for the octonary BioSHEA and quinary BioHEA and was then compared using the following equations [28,29]:

$$\Delta\sigma = \left(\sum \Delta\sigma_i^{3/2}\right)^{2/3}, \qquad (1)$$

$$\Delta\sigma_i = AG_i\delta_i^{4/3}c_i^{2/3}, \qquad (2)$$

where σ_i is the solution strengthening contribution of the i-th element, A is a constant that usually has a value of 0.04, G_i is the shear modulus of the i-th element. The value of δ_i was calculated using the following equations [28,29]:

$$\delta_i = \sqrt{\delta G_i^2 + \beta\delta r_i^2}, \qquad (3)$$

$$\delta r_i = \frac{9}{8}\sum c_j\delta r_{ij}, \qquad (4)$$

$$\delta G_i = \frac{9}{8}\sum c_j\delta G_{ij}, \qquad (5)$$

$$\delta G_{ij} = 2\frac{G_i - G_j}{G_i + G_j}, \qquad (6)$$

$$\delta r_{ij} = 2\frac{r_i - r_j}{r_i + r_j}, \qquad (7)$$

where δG and δr are the shear modulus and atomic size misfit, respectively; β is a constant with a value of 9; δG_{ij} and δr_{ij} are the shear modulus and atomic size misfit between the i-th and j-th elements, respectively. In Eqs. (3)–(7), one element first was considered as the solvent and the rest of the elements were considered as the solutes. Thereafter, the next

element was considered the solvent, and other elements were considered as the solutes. The calculation was thus repeated as many times as the number of constituent elements. Using the G and δ values obtained from the literature (Table 1) [30–32], $\Delta\sigma$ was estimated to be 2292 MPa for TiNbTaZrMoHfWCr BioSHEA and 1604 MPa for TiNbTaZrMo BioHEA. Thus, a higher solid-solution strengthening effect is expected for the BioSHEA.

Fig. 1(c) shows the thermodynamic calculations for the TiNbTaZr-MoHfWCr BioSHEA, which were performed using the Thermocalc software (2022a) and TCHEA5 thermodynamic databases. A body-centered cubic (BCC) solid solution, referred to as BCC1, is expected to form from the liquid phase in the TiNbTaZrMoHfWCr BioSHEA. Fig. 1(d) shows the distribution coefficients (k) of the constituent elements at the liquidus temperature in the TiNbTaZrMoHfWCr BioSHEA, as determined by thermodynamic calculations. The k value of the i-th element (k_i) is defined as the ratio of the concentration of the i-th element in the BCC1 phase ($C_{S,i}$) to that in the liquid phase ($C_{L,i}$), that is, $C_{S,i}/C_{L,i}$, at the liquidus temperature. Elements with relatively high melting points, such as W, Ta, Nb, and Mo, are enriched in the BCC1 phase, whereas elements with low melting points, such as Ti, Zr, Hf, and Cr, exhibit the opposite tendency during solidification (Fig. 1(d)).

Fig. 2(a) shows the XRD patterns obtained from the central region of the arc-melted TiNbTaZrMo BioHEA and TiNbTaZrMoHfWCr BioSHEA ingots and the calculated XRD peak intensities for the C15 intermetallic compound. The peaks in the TiNbTaZrMo BioHEA were indexed to two BCC phases with different lattice constants: a main BCC phase with a lattice constant of 0.329 nm (○) and a minor BCC phase with a lattice constant of 0.341 nm (●) [1]. The TiNbTaZrMoHfWCr BioSHEA exhibited intense peaks corresponding to a BCC1 phase with a lattice constant of 0.326 nm (○) and minor peaks corresponding to a BCC2 phase with a lattice constant of 0.344 nm (●). In addition, peaks corresponding to the precipitated phase were marked (◆). These peaks are consistent with the C15 phase shown in the bottom-part of Fig. 2(a), and the precipitation of C15 phase is predicted from the thermodynamic calculations (Fig. 1(c)). Fig. 2(b) shows the solidification microstructures in the arc-melted ingots. The SEM-backscattered electron (SEM-BSE) images of the central region of the arc-melted TiNbTaZr-MoHfWCr BioSHEA (Fig. 2(b), left panel) indicate a clear solidification microstructure composed of a dendrite (D) region with bright contrast and an interdendrite (ID) region with dark contrast. The results shown in Fig. 1(d) indicate that the elements W, Ta, Nb, and Mo with relatively small atomic radii and averagely large atomic numbers should be enriched in the D region that initially solidified from the liquid phase. The EDS data (Fig. 2(c and d)) essentially capture this trend. BCC1, which shows a higher peak intensity and a smaller lattice constant in the XRD peak profile, corresponds to the D region, as indicated by the relative atomic radii and the volume fraction. In contrast, Ti, Zr, Hf, and Cr enrichment in the ID region and the formation of BCC2 and Laves phases were predicted by equilibrium thermodynamic calculations (Fig. 1(c and d)). As indicated in Fig. 2(b), the ID region was further divided into two phases, referred to as ID-1 and ID-2. ID-1 was enriched in Ti, Zr, Hf with relatively larger atomic radii, which would correspond to BCC2 in the XRD profile with larger lattice constant. Cr was characteristically partitioned to ID-2. Cr exhibits a very large atomic size misfit with Ti, Zr, and Hf. As reported by Hume-Rothery [33], a sufficiently large size mismatch between solvent and solute atoms implies that the solid solution tends to become unstable. Studies evaluating the effect of atomic size mismatch have found, for example, that when Al is included

Table 1

The atomic radius (r), yield strength ($\sigma_{0.2}$), shear modulus (G) of pure metals. These values were used to calculate the solid solution strengthening of BioSHEA [30–32].

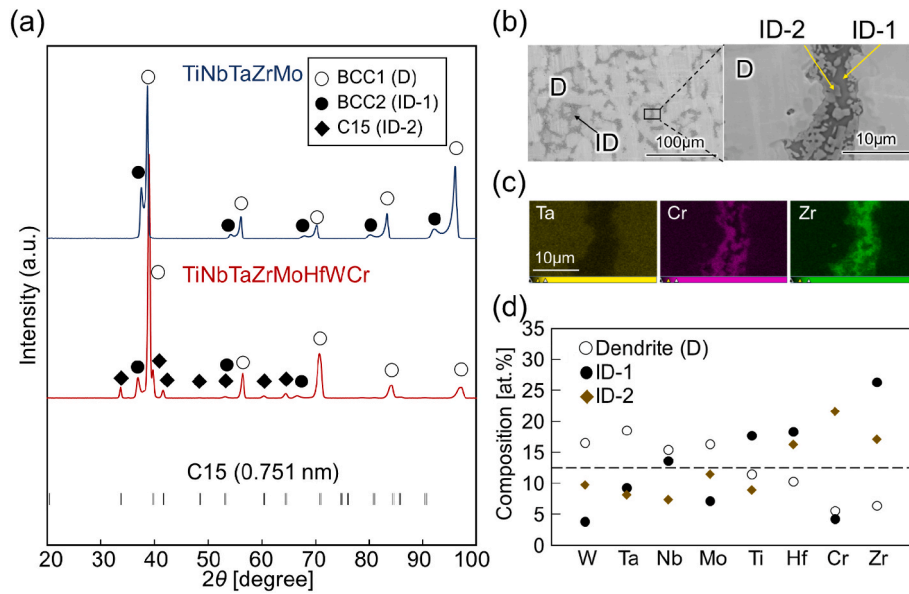| Element	Ti	Zr	Nb	Ta	Mo	Hf	W	Cr
r (Å) [30,31]	1.462	1.603	1.429	1.430	1.363	1.578	1.367	1.249
$\sigma_{0.2}$ (MPa) [30,32]	140	207	105	172	345	230	550	260
G (GPa) [30,31]	45.6	30.0	37.5	69.0	125.5	56.0	160.6	115.1

Fig. 2. Solidification microstructures in the arc-melted ingots of the TiNbTaZrMoHfWCr BioSHEA and TiNbTaZrMo BioHEA. (a) XRD patterns of the arc-melted TiNbTaZrMo BioHEA and TiNbTaZrMoHfWCr BioSHEA and the calculated peaks of the C15-Laves phase. (b) SEM-BSE images and (c) EDS mapping of Ta, Ti, and Zr for the TiNbTaZrMoHfWCr BioSHEA. (d) Chemical composition of the constituent elements obtained from the D, ID-1, and ID-2 regions.

in the alloy, a larger mismatch corresponds to a lower HEA solid solution formation probability [34]. The ID-2 region with enriched Cr as well as Zr and Hf (Fig. 2(d)) corresponded to the C15-Laves phase. The formation of the Cr-rich Laves phase in the ID region as a minor phase is similar to that observed in the Cr-containing TiZrHfCoCrMo BioHEAs [10]. Thus, the arc-melted ingots of the TiNbTaZrMoHfWCr BioSHEA comprise the main W–Ta–Nb–Mo-rich BCC1 dendritic phase and a minor Ti–Zr–Hf–Cr-rich ID region with BCC2 and fine Laves phases.

Fig. 3 shows the biocompatibilities of the arc-melted TiNbTaZr-MoHfWCr BioSHEA, TiNbTaZrMo BioHEA, CP-Ti, and SUS316L. Fluorescent images (Fig. 3(a)) of the cytoskeletal components and focal adhesion of osteoblasts on the specimens indicated that the osteoblasts on the TiNbTaZrMoHfWCr BioSHEA exhibited a widespread morphology with a dense network of actin fibers, which were similar to those on CP-Ti. Fig. 3(b) shows the osteoblast density for the specimens, which was evaluated by Giemsa staining. The cell density of the TiNb-TaZrMoHfWCr BioSHEA (5246 ± 176 cells/cm^2) was comparable to that of CP-Ti (5192 ± 379 cells/cm^2) and TiNbTaZrMo BioHEA (4712 ± 343 cells/cm^2), but significantly higher than that of SUS316L (2835 ± 619 cells/cm^2). No significant differences were observed in the cell areas on the materials (Fig. 3(a)). The alloy design strategy wherein only elements with low biotoxicity were used may have enabled a uniform

spread and tight adhesion of the cells. Thus, the design guideline based on element-specific toxicity was effective for fabricating BioHEAs, even with supermultiple elements.

The mechanical properties of the arc-melted TiNbTaZrMoHfWCr BioSHEA and TiNbTaZrMo BioHEA were compared and the results are shown in Fig. 4. Fig. 4(a) shows the engineering stress–plastic strain curve, and the inset shows 0.2% proof stress (yield strength). The yield strengths of the BioSHEA and BioHEA were 1953 ± 84 MPa and 1402 ± 4 MPa, respectively. The yield strength of the octanary BioSHEA was approximately 550 MPa higher than that of the quinary BioHEA. Assuming a solid solution, the yield stress can be estimated as the sum of average yield strength of the constituent element and the solid solution strengthening [35,36]:

$$\sigma_y^{est} = \sigma_y^{ROM} + \Delta\sigma, \qquad (8)$$

$$\sigma_y^{ROM} = \sum_{i=1}^{n} c_i \sigma_{y,i}, \qquad (9)$$

where σ_y^{est} is the estimated yield strength, σ_y^{ROM} is the yield strength obtained using the rule of mixtures from each constituent element, c_i is the molar fraction of each element, and $\sigma_{y,i}$ is the yield strength of each
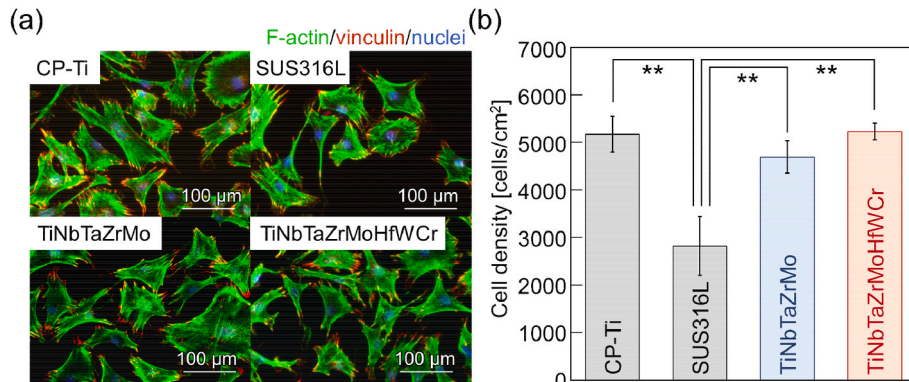

Fig. 3. Biocompatibilities of the arc-melted TiNbTaZrMoHfWCr BioSHEA, CP-Ti, SUS316L, and TiNbTaZrMo BioHEA. (a) Fluorescent staining images. (b) Osteoblast density on the specimens evaluated by Giemsa staining. **: $p < 0.01$.
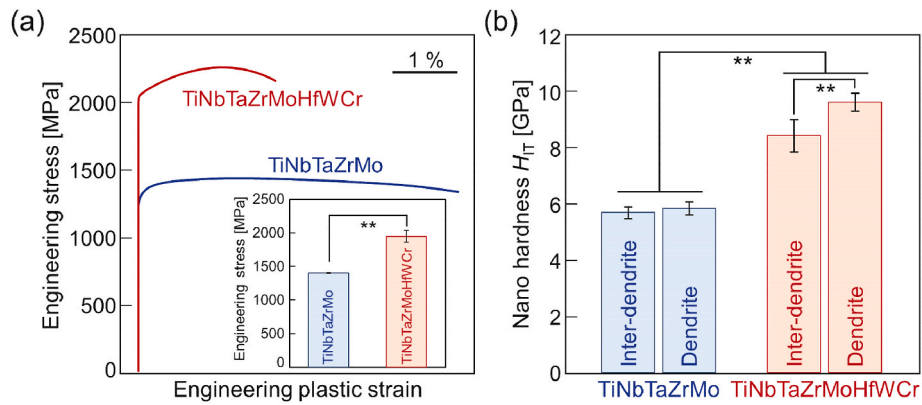
Fig. 4. Mechanical properties of the arc-melted TiNbTaZrMoHfWCr BioSHEA and TiNbTaZrMo BioHEA. (a) Typical engineering stress-engineering plastic strain curves obtained from the compression test at room temperature with an inset showing the yield strength of the TiNbTaZrMo BioHEA and TiNbTaZrMoHfWCr BioSHEA. The data for TiNbTaZrMo BioHEA were reported in Ref. [4]. (b) Nanoindentation hardness at the dendritic and interdendritic regions in the TiNbTaZrMo BioHEA and TiNbTaZrMoHfWCr BioSHEA. **: $p < 0.01$.

constituent element. The $\sigma_{y,i}$ values ranged from 140 MPa (Ti) to 550 MPa (W) [30,32] (Table 1), and the σ_y^{ROM} values varied slightly between the TiNbTaZrMo BioHEA (~200 MPa) and TiNbTaZrMoHfWCr BioSHEA (~260 MPa). Therefore, the significant difference in the yield strength is due to solid-solution strengthening. However, the yield strengths obtained were lower than the calculated values. This might be because the calculation assumes a uniform solid solution of the designed composition without any segregation. However, the alloys fabricated herein were not in the form of a complete single-phase solid solution as represented in Fig. 2. The compositions deviated from equiatomic compositions owing to microsegregation and precipitate formation. Therefore, the strengths of the specimens were lower than the calculated ideal values. Such reductions in the strength from the ideal values owing to compositional deviations have been previously reported [28,37]. To inhibit segregation and develop the original solid-solution strengthening, it is advantageous to fabricate products by laser powder bed fusion, where ultrarapid cooling is possible [13,38]. However, the preparation of alloyed powders using this method is challenging owing to the super-multicomponent system.

Compared with the quinary TiNbTaZrMo BioHEA, the octonary TiNbTaZrMoHfWCr BioSHEA exhibited reduced plastic strain at the cost of high strength. In BCC HEAs, lowering the valence electron concentration (VEC) improves the room temperature ductility [27,39]. In a previous study, we achieved a considerable increase in ductility of quinary BioHEAs by shifting the composition from equiatomic one to reduce VEC [12]. In this study, only the equiatomic composition was examined to elucidate the effects of increase in the number of alloying elements. Improving the ductility of BioSHEA by adjusting the blending ratio of the elements for reduced VEC may be considered in future work.

The ingot exhibited plastic deformation during the compression tests. The presence of a fine Laves phase as a minor phase in the ID region has been reported to be effective in enhancing the mechanical properties of bulk plasticity in Ti alloys [40]. Moreover, a fine Laves phase dispersion in the ID region has been reported to be effective in increasing the hardness of the TiZrHfCoCrMo BioHEA ingots [10]; the TiNbTaZrMoHfWCr BioSHEA may possess a similar mechanism. Fig. 4 (b) shows the nanoindentation hardness of the ID and D regions in the arc-melted TiNbTaZrMo BioHEA and TiNbTaZrMoHfWCr BioSHEA. For the TiNbTaZrMoHfWCr BioSHEA, the nanoindentation hardness in the ID region was obtained from a mixture of ID-1 and ID-2 regions (Fig. 2 (b)). The nanoindentation hardnesses for the ID and D regions of the TiNbTaZrMo BioHEA were 5.67 GPa and 5.82 GPa, respectively, while those for the TiNbTaZrMoHfWCr BioSHEA were 8.40 GPa and 9.61 GPa, respectively. The nanoindentation hardness in the D region of the Bio-SHEA without the precipitated phase was significantly higher than those

in the main BCC dendritic and minor BCC interdendritic regions of the BioHEA. This indicates that a solid-solution strengthening effect occurs in the D region (BCC1 phase) via elemental interactions in the BioSHEA. In accordance with Eqs. (1)–(7), the significantly higher hardness in the D region of the TiNbTaZrMoHfWCr BioSHEA than that in the ID region was attributed to the higher shear moduli of the concentrated elements, primarily W, Mo, and Ta.

Solid-solution strengthening is widely recognized as a predominant mechanism responsible for the exceptionally high strength of HEAs with similar compositions of SHEA reported in thus study such as (TiZrNbTa)–Mo [41] and TaNbHfZrTi [28,42]. Moreover, the BioSHEA reported in this study showed Laves phase. The strengthening effect of Laves phase dispersion in HEAs has been previously reported [10]. Other possible contributions from nanoscale phase separation, short range order, and fine precipitates have not been considered in this analysis. The contributions from these effects must be analyzed using transmission electron microscopy and scanning transmission electron microscopy, which is a challenge for future work.

In addition to high biocompatibility, biomaterials used in bone implants should exhibit excellent mechanical properties. In particular, joint replacement implants induce relative motion between mating parts and should withstand wear on the mating surfaces [43]. Since hardness is strongly correlated with wear resistance, these results suggest that super-multicomponent BioSHEA may exhibit good wear resistance.

In this study, a metallic biomaterial with high strength as well as good biocompatibility was obtained via super-multicomponentization. A high strength allows for a reduction in the cross-sectional area of the implant (e.g., bone plate) to meet the mechanical requirements, which in turn allows for a reduction in the stiffness of the implant. Thus, it can contribute to the inhibition of stress shielding to the bone [44]. Furthermore, the toxicity of metal ions to living organisms is not a linear function of ion concentration, but increases considerably at certain concentrations [19]. This means that even elements with a marginally lower biocompatibility than Ti, such as W and Cr, which may be toxic at high concentrations, can be used in the non-toxic range. Therefore, "super-high-entropy" is an effective strategy to increase the strength of metallic biomaterials while maintaining their biocompatibility.

4. Conclusion

This study clarified that an increase in entropy from BioHEA to BioSHEA was significantly effective in increasing the mechanical strength via solid-solution hardening. Moreover, BioSHEA exhibited excellent biocompatibility, which was comparable to that of CP-Ti and BioHEA. In conclusion, this study demonstrated the concept of SHEAs for application as metallic biomaterials (BioSHEAs) with $\Delta S_{mix} \geq 2.0R$

and the development of the TiNbTaZrMoHfWCr BioSHEA. The main constituent phase of the BioSHEA ingot was the BCC phase, with minor Laves phases. The biocompatibility of the BioSHEA was comparable to that of CP-Ti and previously reported BioHEAs. The mechanical strength of BioSHEA was significantly higher than that of BioHEA owing to the solid-solution hardening of the BCC phase and the fine Laves phase dispersion. Thus, the developed strategy involving an increase in the entropy of HEAs serves as a novel entropy-based guideline for the development of a new class of metallic biomaterials.

Funding

Data statement

Data will be made available on request.

CRediT authorship contribution statement

Tadaaki Matsuzaka: Formal analysis, Methodology, Visualization, Writing – original draft. **Akira Hyakubu:** Formal analysis, Investigation, Methodology, Software, Visualization. **Yong Seong Kim:** Software, Visualization. **Aira Matsugaki:** Methodology, Supervision, Validation, Writing – review & editing. **Takeshi Nagase:** Investigation, Methodology, Software, Validation, Writing – review & editing. **Takuya Ishimoto:** Methodology, Supervision, Validation, Writing – review & editing. **Ryosuke Ozasa:** Investigation, Methodology, Supervision. **Hyoung Seop Kim:** Investigation, Methodology, Supervision. **Tomoji Mizuguchi:** Investigation, Supervision. **Ozkan Gokcekaya:** Investigation, Supervision. **Takayoshi Nakano:** Conceptualization, Funding acquisition, Project administration, Resources, Supervision, Validation, Writing – review & editing.

Declaration of competing interest

The authors declare that they have no known competing financial interests or personal relationships that could have appeared to influence the work reported in this paper.

References

[1] J.-W. Yeh, S.-K. Chen, S.-J. Lin, J.-Y. Gan, T.-S. Chin, T.-T. Shun, C.-H. Tsau, S.-Y. Chang, Nanostructured high-entropy alloys with multiple principal elements: novel alloy design concepts and outcomes, Adv. Eng. Mater. 6 (2004) 299–303, https://doi.org/10.1002/adem.200300567.

[2] J.W. Yeh, S.Y. Chang, Y.D. Hong, S.K. Chen, S.J. Lin, Anomalous decrease in X-ray diffraction intensities of Cu–Ni–Al–Co–Cr–Fe–Si alloy systems with multi-principal elements, Mater. Chem. Phys. 103 (2007) 41–46, https://doi.org/10.1016/j.matchemphys.2007.01.003.

[3] B. Cantor, Multicomponent and high entropy alloys, Entropy 16 (2014) 4749–4768, https://doi.org/10.3390/e16094749.

[4] M. Todai, T. Nagase, T. Hori, A. Matsugaki, A. Sekita, T. Nakano, Novel TiNbTaZrMo high-entropy alloys for metallic biomaterials, Scripta Mater. 129 (2017) 65–68, https://doi.org/10.1016/j.scriptamat.2016.10.028.

[5] S.P. Wang, J. Xu, TiZrNbTaMo high-entropy alloy designed for orthopedic implants: as-cast microstructure and mechanical properties, Mater. Sci. Eng. C 73 (2017) 80–89, https://doi.org/10.1016/j.msec.2016.12.057.

[6] T. Nagase, M. Todai, T. Hori, T. Nakano, Microstructure of equiatomic and non-equiatomic Ti-Nb-Ta-Zr-Mo high-entropy alloys for metallic biomaterials, J. Alloys Compd. 753 (2018) 412–421, https://doi.org/10.1016/j.jallcom.2018.04.082.

[7] A. Motallebzadeh, N.S. Peighambardoust, S. Sheikh, H. Murakami, S. Guo, D. Canadinc, Microstructural, mechanical and electrochemical characterization of TiZrTaHfNb and Ti₁.₅ZrTa₀.₅Hf₀.₅Nb₀.₅ refractory high-entropy alloys for biomedical applications, Intermetallics 113 (2019) 106572, https://doi.org/10.1016/j.intermet.2019.106572.

[8] Y. Yuan, Y. Wu, Z. Yang, X. Liang, Z. Lei, H. Huang, H. Wang, X. Liu, K. An, W. Wu, Z. Lu, Formation, structure and properties of biocompatible TiZrHfNbTa high-entropy alloys, Mater. Res. Lett. 7 (2019) 225–231, https://doi.org/10.1080/21663831.2019.1584592.

[9] T. Hori, T. Nagase, M. Todai, A. Matsugaki, T. Nakano, Development of non-equiatomic Ti–Nb–Ta–Zr–Mo high-entropy alloys for metallic biomaterials, Scripta Mater. 172 (2019) 83–87, https://doi.org/10.1016/j.scriptamat.2019.07.011.

[10] T. Nagase, Y. Iijima, A. Matsugaki, K. Ameyama, T. Nakano, Design and fabrication of Ti–Zr–Hf–Cr–Mo and Ti–Zr–Hf–Co–Cr–Mo high-entropy alloys as metallic biomaterials, Mater. Sci. Eng. C 107 (2020) 110322, https://doi.org/10.1016/j.msec.2019.110322.

[11] G. Perumal, H.S. Grewal, M. Pole, L.V.K. Reddy, S. Mukherjee, H. Singh, G. Manivasagam, H.S. Arora, Enhanced biocorrosion resistance and cellular response of a dual-phase high entropy alloy through reduced elemental heterogeneity, ACS Appl. Bio Mater. 3 (2020) 1233–1244, https://doi.org/10.1021/acsabm.9b01127.

[12] Y. Iijima, T. Nagase, A. Matsugaki, P. Wang, K. Ameyama, T. Nakano, Design and development of Ti–Zr–Hf–Nb–Ta–Mo high-entropy alloys for metallic biomaterials, Mater. Des. 202 (2021) 109548, https://doi.org/10.1016/j.matdes.2021.109548.

[13] T. Ishimoto, R. Ozasa, K. Nakano, M. Weinmann, C. Schnitter, M. Stenzel, A. Matsugaki, T. Nagase, T. Matsuzaka, M. Todai, H.S. Kim, T. Nakano, Development of TiNbTaZrMo bio-high entropy alloy (BioHEA) super-solid solution by selective laser melting, and its improved mechanical property and biocompatibility, Scripta Mater. 194 (2021) 113658, https://doi.org/10.1016/j.scriptamat.2020.113658.

[14] T. Xiang, P. Du, Z. Cai, K. Li, W. Bao, X. Yang, G. Xie, Phase-tunable equiatomic and non-equiatomic Ti–Zr–Nb–Ta high-entropy alloys with ultrahigh strength for metallic biomaterials, J. Mater. Sci. Technol. 117 (2022) 196–206, https://doi.org/10.1016/j.jmst.2021.12.014.

[15] T. Nagase, M. Matsumoto, Y. Fujii, Microstructure of Ti–Ag immiscible alloys with liquid phase separation, J. Alloys Compd. 738 (2018) 440–447, https://doi.org/10.1016/j.jallcom.2017.12.138.

[16] T. Nagase, K. Mizuuchi, T. Nakano, Solidification microstructures of the ingots obtained by arc melting and cold crucible levitation melting in TiNbTaZr medium-entropy alloy and TiNbTaZrX (X = V, Mo, W) high-entropy alloys, Entropy 21 (2019) 483, https://doi.org/10.3390/e21050483.

[17] W.C. Oliver, G.M. Pharr, An improved technique for determining hardness and elastic modulus using load and displacement sensing indentation experiments, J. Mater. Res. 7 (1992) 1564–1583, https://doi.org/10.1557/JMR.1992.1564.

[18] M. Niinomi, Recent metallic materials for biomedical applications, Metall. Mater. Trans. 33 (2002) 477–486, https://doi.org/10.1007/s11661-002-0109-2.

[19] A. Yamamoto, R. Honma, M. Sumita, Cytotoxicity evaluation of 43 metal salts using murine fibroblasts and osteoblastic cells, J. Biomed. Mater. Res. 39 (1998) 331–340, https://doi.org/10.1002/(SICI)1097-4636(199802)39:2<331::AID-JBM22>3.0.CO;2-E.

[20] J.W. Yeh, Alloy design strategies and future trends in high-entropy alloys, JOM 65 (2013) 1759–1771, https://doi.org/10.1007/s11837-013-0761-6.

[21] B.S. Murty, J.W. Yeh, S. Ranganathan, P.P. Bhattacharjee, High-entropy Alloys, Elsevier, 2019.

[22] M.C. Gao, J.W. Yeh, P.K. Liaw, Y. Zhang, High-entropy Alloys: Fundamentals and Applications, Springer, 2016.

[23] Y.F. Ye, Q. Wang, J. Lu, C.T. Liu, Y. Yang, High-entropy alloy: challenges and prospects, Mater. Today 19 (2016) 349–362, https://doi.org/10.1016/j.mattod.2015.11.026.

[24] Y. Zhang, Z.P. Lu, S.G. Ma, P.K. Liaw, Z. Tang, Y.Q. Cheng, M.C. Gao, Guidelines in predicting phase formation of high-entropy alloys, MRS Commun. 4 (2014) 57–62, https://doi.org/10.1557/mrc.2014.11.

[25] A. Takeuchi, A. Inoue, Calculations of mixing enthalpy and mismatch entropy for ternary amorphous alloys, Mater. Trans., JIM 41 (2000) 1372–1378, https://doi.org/10.2320/matertrans1989.41.1372.

[26] X. Yang, Y. Zhang, Prediction of high-entropy stabilized solid-solution in multi-component alloys, Mater. Chem. Phys. 132 (2012) 233–238, https://doi.org/10.1016/j.matchemphys.2011.11.021.

[27] S. Sheikh, S. Shafeie, Q. Hu, J. Ahlström, C. Persson, J. Veselý, J. Zýka, U. Klement, S. Guo, Alloy design for intrinsically ductile refractory high-entropy alloys, J. Appl. Phys. 120 (2016) 164902, https://doi.org/10.1063/1.4966659.

[28] O.N. Senkov, J.M. Scott, S.V. Senkova, D.B. Miracle, C.F. Woodward, Microstructure and room temperature properties of a high-entropy TaNbHfZrTi alloy, J. Alloys Compd. 509 (2011) 6043–6048, https://doi.org/10.1016/j.jallcom.2011.02.171.

[29] I. Toda-Caraballo, P.E.J. Rivera-Díaz-del-Castillo, Modelling solid solution hardening in high entropy alloys, Acta Mater. 85 (2015) 14–23, https://doi.org/10.1016/j.actamat.2014.11.014.

[30] F. Cardarelli, Materials Handbook: a Concise Desktop Reference, second ed., Springer, London, 2008.

[31] V.A. Lubarda, On the effective lattice parameter of binary alloys, Mech. Mater. 35 (2003) 53–68, https://doi.org/10.1016/S0167-6636(02)00196-5.

[32] U. Holzwarth, H. Stamm, Mechanical and thermomechanical properties of commercially pure chromium and chromium alloys, J. Nucl. Mater. 300 (2002) 161–177, https://doi.org/10.1016/S0022-3115(01)00745-0.

[33] W. Hume-Rothery, G.W. Mabbott, K.M.C. Evans, The freezing points, melting points, and solid solubility limits of the alloys of silver and copper with the elements of the B sub-groups, Philos. Trans. R. Soc. London, A 233 (1934) 1–97, https://doi.org/10.1098/rsta.1934.0014.

[34] E.J. Pickering, N.G. Jones, High-entropy alloys: a critical assessment of their founding principles and future prospects, Int. Mater. Rev. 61 (2016) 183–202, https://doi.org/10.1080/09506608.2016.1180020.

[35] H.W. Yao, J.W. Qiao, J.A. Hawk, H.F. Zhou, M.W. Chen, M.C. Gao, Mechanical properties of refractory high-entropy alloys: experiments and modeling, J. Alloys Compd. 696 (2017) 1139–1150, https://doi.org/10.1016/j.jallcom.2016.11.188.

[36] Y. Di, M. Wang, L. Zhang, H. Yan, Y. Zhang, Y. Lu, A novel $Ti_{45}V_{45}(AlCrMo)_{10}$ lightweight medium-entropy alloy with outstanding mechanical properties, Mater. Lett. 339 (2023) 134089, https://doi.org/10.1016/j.matlet.2023.134089.

[37] W. Zheng, S. Lü, S. Wu, X. Chen, W. Guo, Development of $MoNbVTa_x$ refractory high entropy alloy with high strength at elevated temperature, Mater. Sci. Eng., A 850 (2022) 143554, https://doi.org/10.1016/j.msea.2022.143554.

[38] O. Gokcekaya, T. Ishimoto, Y. Nishikawa, Y.S. Kim, A. Matsugaki, R. Ozasa, M. Weinmann, C. Schnitter, M. Stenzel, H.S. Kim, Y. Miyabayashi, T. Nakano, Novel single crystalline-like non-equiatomic TiZrHfNbTaMo bio-high entropy alloy (BioHEA) developed by laser powder bed fusion, Mater. Res. Lett. 11 (2023) 274–280, https://doi.org/10.1080/21663831.2022.2147406.

[39] T. Yang, Y.L. Zhao, W.H. Liu, J.H. Zhu, J.J. Kai, C.T. Liu, Ductilizing brittle high-entropy alloys via tailoring valence electron concentrations or precipitates by controlled elemental partitioning, Mater. Res. Lett. 6 (2018) 600–606, https://doi.org/10.1080/21663831.2018.1518276.

[40] C.D. Rabadia, Y.J. Liu, L.Y. Chen, S.F. Jawed, L.Q. Wang, H. Sun, L.C. Zhang, Deformation and strength characteristics of Laves phases in titanium alloys, Mater. Des. 179 (2019) 107891, https://doi.org/10.1016/j.matdes.2019.107891.

[41] S.-P. Wang, J. Xu, (TiZrNbTa)-Mo high-entropy alloys: Dependence of microstructure and mechanical properties on Mo concentration and modeling of solid solution strengthening, Intermetallics 95 (2018) 59–72, https://doi.org/10.1016/j.intermet.2018.01.017.

[42] O.N. Senkov, G.B. Wilks, D.B. Miracle, C.P. Chuang, P.K. Liaw, Refractory high-entropy alloys, Intermetallics 18 (2010) 1758–1765, https://doi.org/10.1016/j.intermet.2010.05.014.

[43] L. Kunčická, R. Kocich, T.C. Lowe, Advances in metals and alloys for joint replacement, Prog. Mater. Sci. 88 (2017) 232–280, https://doi.org/10.1016/j.pmatsci.2017.04.002.

[44] A. Chmielewska, D. Dean, The role of stiffness-matching in avoiding stress shielding-induced bone loss and stress concentration-induced skeletal reconstruction device failure, Acta Biomater. 173 (2024) 51–65, https://doi.org/10.1016/j.actbio.2023.11.011.